White Rose
university consortium
Universities of Leeds, Sheffield & York

eprints@whiterose.ac.uk
https://eprints.whiterose.ac.uk/

Decoration of plasmonic Mg nanoparticles

by partial galvanic replacement

Jérémie Asselin[1,2], Christina Boukouvala[1,2], Yuchen Wu[1], Elizabeth R. Hopper[1,2,3], Sean M.

Collins[1], John S. Biggins[4], Emilie Ringe[1,2]*

1. Department of Materials Science and Metallurgy, University of Cambridge, Cambridge, United Kingdom, CB3 0FS

2. Department of Earth Sciences, University of Cambridge, Downing Street, Cambridge, United Kingdom, CB2 3EQ

3. Department of Chemical Engineering and Biotechnology, University of Cambridge, Cambridge, United Kingdom, CB3 0AS

4. Department of Engineering, University of Cambridge, Trumpington Street, Cambridge, United Kingdom, CB2 1PZ

* Corresponding author: er407@cam.ac.uk; +44 (0)1223 334300 (ph.), +44 (0)1223 334567 (fax).

ABSTRACT

Plasmonic structures have attracted much interest in science and engineering disciplines, exploring a myriad of potential applications owing to their strong light-matter interactions. Recently, the plasmonic concentration of energy in sub-wavelength volumes has been used to initiate chemical reactions, for instance by combining plasmonic materials with catalytic metals. In this work, we demonstrate that plasmonic nanoparticles of earth-abundant Mg can undergo galvanic replacement in a non-aqueous solvent to produce decorated structures. This method yields bimetallic architectures where partially oxidized 200-300 nm Mg nanoplates and nanorods support many smaller Au, Ag, Pd or Fe nanoparticles, with potential for a stepwise process introducing multiple decoration compositions on a single Mg particle. We investigated this mechanism by electron-beam imaging and local composition mapping with energy-dispersive X-ray spectroscopy (EDS) as well as, at the ensemble level, by inductively coupled plasma mass spectrometry (ICP-MS). High-resolution scanning transmission electron microscopy (HR-STEM) further supported the bimetallic nature of the particles and provided details of the interface geometry, which includes a Mg oxide separation layer between Mg and the other metal. Depending on the composition of the metallic decorations, strong plasmonic optical signals characteristic of plasmon resonances were observed in the bulk with UV-Vis spectrometry and at the single particle level with darkfield scattering. These novel bi- and multimetallic designs open up an exciting array of applications where one or multiple plasmonic structures could interact in the near-field of earth-abundant Mg, and couple with catalytic nanoparticles for applications in sensing and plasmon-assisted catalysis.

I. INTRODUCTION

The strong light-matter interactions afforded by plasmonic nanoparticles (NPs) have found a plethora of applications ranging from photothermal cancer therapy[1] to enhanced spectroscopies[2–4], from light-enhanced catalysis[5,6] to switchable displays[7,8], and much more.[9,10] Traditional plasmonic materials include Ag and Au but, recently, the quest for cheaper, more sustainable materials led to the prediction[11,12] and experimental realization[7,13–19] of plasmonic structures based on Cu, Al, and Mg. While the development of such plasmonic structures is still in its infancy compared to those of Ag and Au, significant recent advances position these earth-abundant materials firmly into the plasmonic toolbox. For example, better understanding of the nucleation mechanism of Al NPs has improved synthetic control over their size, shape and reaction yield,[13–15,18,20] while the comparatively less explored Mg[11,21,22] has just recently been synthesized colloidally.

Both Al and Mg present interesting optical, chemical and physical properties that complement those of noble metal structures, including accessing different spectral ranges and different surface chemistries. Indeed, the dielectric function of Mg displays relatively low losses across the ultraviolet-visible-near infrared (UV-Vis-NIR) wavelength range, making it an attractively flexible platform. Further, its hexagonal close packed (*hcp*) crystal structure, distinct from the typical face-centered cubic (*fcc*) structure of the common plasmonic metals (Au, Ag, Cu, Al), unlocks a variety of potential thermodynamic and kinetic shapes, for both single crystalline and twinned structures.

Mg plasmonics have been only recently demonstrated. Blair *et al.* experimentally confirmed the presence of Mg plasmons in a thin film nanohole array and compared its response to Al samples.[23] Further lithographic work by Sterl *et al.* showed the switching between plasmonic and non-

plasmonic behavior as metallic Mg is reduced to the dielectric MgH_2 by hydrogen gas.[24] Recently, Biggins, Yazdi, and Ringe[25] adapted an electroless synthesis[26] to prepare colloidal Mg hexagonal nanoplates, and described, experimentally and numerically, their LSPR activity across the UV-Vis-NIR range. Through our studies of Mg metal synthesis, a key challenge has been its large negative reduction potential (ΔE= -2.37 V, SHE),[27] making Mg prone to spontaneous oxidation and demanding strictly controlled synthesis conditions, much like Al.[28] This prevents the use of "typical" (used for Ag, Au) reducing agents and surfactants, and is further exacerbated in NP form owing to their large surface to volume ratio. Despite this unlikely stability, Mg and Al NPs do exist in the metallic form, protected, in air or in dry solvents, by a thin (5-20 nm) oxide layer; they both react immediately in water to fully oxidize unless otherwise protected.[13,22,29,30]

An upside of this reduction potential is the strong thermodynamic driving force for reactions such as galvanic replacement, where a more easily reduced ion (i.e., less easily oxidized, more noble) takes electrons from Mg metal to generate both Mg ions and a metallic form of the aforementioned ion. This spontaneous reaction has seldom been used for Mg; an example of which is its reaction to form porous, rough Au or Ag nanoshells from laser-ablated particles.[31,32] Meanwhile, galvanic replacement has been wildly successful at producing interesting and complex plasmonic structures, mainly based on Au, Pd, or Pt, functionalization of different Ag (semi-)sacrificial templates mostly in water,[33–35] but sometimes in organic solvents.[36–42] This is a mature approach for AgAu hollow systems, where the extent of galvanic replacement and alloying can be controlled by not only stoichiometry, but also the addition of reducing agents.[43]

Here, we show that stoichiometry-controlled partial galvanic replacement leads to the tunable decoration of well defined, crystalline, Mg NPs with Au, Ag, Pd and Fe. Composition mapping and elemental analyses confirm the galvanic replacement mechanism, and advanced electron

microscopy techniques and single-particle scattering measurements further unravel the bimetallic and plasmonic nature of the particles. Unlike the crystallographic compatibility and miscibility of *fcc*-based noble metals,[44,45] the *hcp* lattice of Mg supports immiscible smaller metal nanoparticles on a thin MgO layer.

II. MATERIALS AND METHODS

A. CHEMICALS AND REAGENTS

Di-*n*-butylmagnesium (1.0 M in heptane), lithium, naphthalene, anhydrous tetrahydrofuran (THF), tetraethyl orthosilicate (TEOS), triethylamine, potassium gold(III) chloride (KAuCl$_4$), potassium tetrachloropalladate(II) (Na$_2$PdCl$_4$), silver nitrate (AgNO$_3$, 99%), and iron(III) chloride (FeCl$_3$) were purchased from Sigma-Aldrich. Anhydrous isopropanol (IPA) was obtained from Fisher Scientific. Unless otherwise stated, anhydrous ethanol (VWR) was used as a solvent for centrifugation steps, and all chemical reagents were used without further purification. All synthesis glassware was washed with aqua regia (1:3 HNO$_3$:HCl) and flame-dried under vacuum. (*Caution: Aqua regia solutions are dangerous and should be used with extreme care; these solutions should never be stored in closed containers.*)

B. SYNTHESIS OF DECORATED Mg NANOPARTICLES

Mg NPs were prepared by the reduction of di-*n*-butylmagnesium by a lithium naphthalenide complex following a previously reported procedure.[25] Briefly, 2.12 g of naphthalene, 0.112 g of lithium, and 20 mL of anhydrous THF were added to a Schlenk flask under Ar atmosphere, and then sonicated for 1 hour in a sealed vial. Additional anhydrous THF (23 mL), then di-*n*-butylmagnesium in heptane (1.0 M, 7 mL) were added under Ar atmosphere, and left to stir

5

vigorously over 16 hours with a glass stirring bar. The reaction was quenched by injecting 20 mL of IPA, and the mixture was purified by successive centrifugation steps in THF (once) and IPA (twice). Further cleaning of the Mg nanoplates was achieved by a surface reaction methodology. A suspension of Mg NPs (1.5 mL) was diluted with 11.0 mL of ethanol before adding 0.9 mL of a TEOS solution (20 μL TEOS in 5 mL ethanol, 9 mM) and 0.3 mL of triethylamine, and left to react under stirring for at least 16-20 hours. Samples were purified twice by centrifugation in ethanol before being resuspended in 3.0 mL of anhydrous ethanol. No silica shells were observed in either imaging or elemental mapping.

The Mg content of the purified samples was determined by inductively coupled plasma mass spectrometry (ICP-MS). This concentration was used to determine the amount of metal salt to be added for the galvanic replacement in order to obtain a specific stoichiometry. In a typical decoration experiment, the NP suspension was diluted to 2.4 mM (Mg concentration) with anhydrous ethanol before the dropwise addition of different volumes of a 2.4 mM anhydrous solution in ethanol of $KAuCl_4$, $AgNO_3$, $FeCl_3$, or Na_2PdCl_4 under vigorous stirring. Suspensions were diluted with ethanol to normalize the Mg concentration in all samples at 1.2 mM. Samples were left to react over 16 hours, unless otherwise stated, before further characterization. Control experiments with the same Au, Ag, Fe, and Pd salts dissolved in ethanol showed stable absorbance values over 24 hours, without formation of small metallic NPs. Likewise, Mg NPs suspended in anhydrous ethanol did not spontaneously dissolve or oxidize, and their extinction value remained unchanged after 24 hours or indeed several weeks.

C. CHARACTERIZATION

Samples were drop cast on Si wafers for SEM imaging performed on a Quanta-650F Field Emission Gun Scanning Electron Microscope. All TEM, STEM, STEM-EELS, STEM-EDS, and associated data presented in the manuscript were acquired at 200 kV on a FEI Osiris S/TEM equipped with a Bruker Super-X quad EDS detector, and a Gatan Enfinium ER 977 electron spectrometer. TEM and STEM analyses were performed on NPs drop cast on an ultrathin carbon membrane deposited on a lacey carbon Cu TEM grid and rinsed with ethanol. Aberration corrected high resolution scanning transmission electron microscopy (HR-STEM) was performed using a JEOL ARM300CF microscope equipped with a cold field emission electron source and JEOL aberration correctors in both the probe-forming and image-forming optics, located in the electron Physical Sciences Imaging Centre (ePSIC) at the Diamond Light Source. The microscope was operated at 300 kV with a convergence semi-angle of approximately 33 mrad. Micrographs were recorded using the annular bright field (ABF) STEM signals from an ABF aperture and a bright field detector, with a camera length selected such that the outer edge of the direct beam disk was aligned with the outer edge of the ABF aperture.

The samples were prepared in air for galvanic replacement experiments using anhydrous solvents and analyzed promptly (less than two days after the reaction). STEM-EDS maps were obtained by integrating the K_α lines of Mg (1.25 eV) and O (0.53 eV), and the L_α lines of Au (9.71 eV) and Ag (2.98 eV). Extinction spectra were obtained on a Perkin-Elmer Lambda 750 UV-Vis-NIR spectrophotometer. Darkfield optical scattering spectra were obtained on an optical microscope equipped with a halogen lamp, darkfield condenser (NA 0.85−0.95), 100× oil immersion objective (NA 1.3), Princeton Instruments Isoplane spectrometer (50 grooves/mm) and ProEM 1024 × 1024 pixels EMCCD.[46]

III. RESULTS AND DISCUSSION

A. Mg NANOPARTICLES SYNTHESIS AND CHARACTERIZATION

Plasmonic Mg NPs were synthesized using a previously reported approach.[25] Briefly, di-*n*-butylmagnesium was reduced by a lithium naphthalenide complex in dry tetrahydrofuran (THF) under an Ar atmosphere. The reaction mixture was then quenched with isopropanol (IPA), centrifuged, and dispersed in anhydrous THF and IPA, successively. The resulting hexagonal Mg NPs have an average length, tip-to-tip, of 260±80 nm and a thickness of 36±7 nm (Figure S1). The reaction mixture, shown in Figure 1A, also includes a significant number of truncated triangles as well as rods, interesting crystalline products which we are currently investigating in more depth. The reaction yield consists of 45% hexagonal nanoplates, 15% truncated triangles and 40% nanorods with various aspect ratio. Despite this variability in size and shape, all particles comprise a Mg core protected by a ~6-8 nm thick Mg oxide layer as shown by elemental mapping in Figures 1C and S2; this passivation layer prevents further oxidation of the core. Mg was confirmed to be metallic by the observation, in scanning transmission electron microscopy electron energy loss spectroscopy (STEM-EELS), of both the presence of a bulk metallic plasmon at 10.6 eV and the characteristic hydrogenic shape of the metallic Mg K-edge at 1.3 keV (Figure S3).

Figure 1.   A) Representative scanning electron micrograph (SEM) of bare Mg NPs, the starting point for galvanic replacement. B) High-angle annular darkfield STEM (HAADF-STEM) of a single hexagonal nanoplate. C) STEM energy dispersive X-ray spectroscopy (STEM-EDS) elemental map showing the Mg K_α and O K_α signals,

pixel: 4.5×4.5 nm (inset: higher-resolution image of the Mg/MgO interface, pixel: 2×2 nm), scalebar, 100 nm.

Mg NPs in suspension have a plasmonic band peaking broadly near and above 800 nm (Figure S4). This wide extinction signature is notably influenced by the sample's size polydispersity, shape heterogeneity, and fluctuations in the thickness of the oxide layer. The former was investigated in-depth in our previous publication,[25] while numerical data supporting the latter is reported in Figure S5. These variations in peak position are then compounded by the fact that each nanoplate sustains multiple modes spanning the UV-Vis-NIR. To surmount this heterogeneous broadening, the optical signature of single particles can be analyzed using a darkfield microscope. A dominant scattering mode, the dipolar mode, was observed at 630 nm or higher for particles confirmed to be single by SEM.[25] A change in refractive index for substrate-supported NPs compared to colloidal ones (suspended in ethanol) explains most of the dipolar energy discrepancy between the single-particle (> 630 nm) and the ensemble (800 nm) measurements.

B. Au-DECORATED Mg NANOPARTICLES

Figure 2.   HAADF-STEM images and EDS maps for Mg K_α, O K_α, and Au L_α signals from A) hexagonal Mg NPs with high coverage of Au decorations, and from Mg nanorods decorated at different locations on their length (B: tip, C: twice in the middle). Scalebars, 100 nm.

An obvious candidate for a galvanic replacement reaction is Au, given its noble character, resistance to oxidation, well characterized plasmonic properties, and abundant previous reports of

reaction with Ag.[38,40,41,43] There is not a straightforward analogy between Au/Ag and Au/Mg. Indeed, whereas Ag and Au have similar *fcc* crystal lattices, Mg crystallizes in a *hcp* structure. Unlike AgAu alloys,[47] neither Au nor Ag are miscible at any concentrations with Mg,[48,49] and their lattice mismatch [Mg *a*=0.321, *c*=0.521 nm, Au *a*=0.408 nm and Ag 0.409] suggests a non-mixing behavior. This is further supported by the discrepancy between the atomic distances within their close-packed planes, i.e. the {001} plane in Mg (0.321 nm) and the {111} in Au (0.288 nm).

The addition of anhydrous $KAuCl_4$ to Mg NPs in ethanol produces small gold decorations (Figure 2). Control experiments involving the dissolution of Au salt or the dispersion of Mg NPs in anhydrous ethanol did not induce spontaneous reduction or oxidation reactions, respectively. The high atomic number (Z) of Au compared to Mg creates a distinctive difference in signal intensities in both HAADF-STEM and SEM, often making it difficult to observe the Mg NPs without the Au decorations being very bright. STEM-EDS mapping of decorated MgAu NPs reveals a sharp decrease of the Mg K_α intensity, while the O K_α signal remains comparable in representative particles before and after oxidation; the ratio of Mg to O signal notably decreases. Interestingly, upon galvanic replacement of Mg nanorods by Au, most of the Mg signal decreases in the vicinity of noble metal decorations (i.e. where electrons were used), leaving a stronger intensity away along the longitudinal axis. Figures 2B and 2C illustrate this depletion effect when Au decorations are located at the tip and in the middle, respectively.

Since the Au decorations are clustered on the Mg particle and neither survey SEM nor STEM images of drop-cast reaction mixtures show free, unbound Au NPs (Figure S6), we hypothesize that the MgO surface supports and retains the smaller metallic decorations. Decades ago, Marks presented evidence that shows a reorganization of MgO around small Au NPs to minimize surface energy at the point of contact.[50] Here, high-resolution STEM of the Mg/MgO/Au interface confirm

that the noble metal decorations are in contact with the 5-nm thick MgO layer (Figure 3). Fast Fourier transform (FFT) of these regions further supports the distinction between the hexagonal packing of Mg (3.0 Å, {102} spacing) and the cubic arrangement of MgO (2.1 Å, {200} spacing).

Figure 3.   ABF-STEM images of A) Au-decorated Mg nanoplates and B) the Mg/MgO/Au interface. Inset: FFT of selected Mg (3.0 Å, corresponding to the {102} spacing) and MgO (2.1 Å, corresponding to {200} spacing) from the regions of interest indicated in the main image.

Despite the presence, confirmed by HR-STEM and STEM-EDS, of a continuous oxide layer on the Mg NPs, both before and after decoration, partial galvanic replacement convincingly occurs to yield small Au NPs. The solvent, ethanol, does not act as a reducing agent, a claim supported by three observations: 1) our procedure happens at room temperature, 2) no reduction is observed for metal salts in ethanol without Mg NPs, and 3) Au NPs are always seen attached to Mg NPs. No other agents or surfactants are added to the solution. Further, the loss of Mg signal both in EDS (Mg K_α peak, Figure S7) and in EELS (K-edge shape change, Figure S8) upon oxidation, along with further evidence discussed below, solidly anchor the galvanic replacement mechanism. The behavior of the oxide layer during reaction remains unclear, but a plausible hypothesis is that small defects and thinner regions act as "weak" spots for the nucleation of Au NPs and exchange of electrons; these are potentially healed later by the growth of a more uniform oxide layer upon exposure to air. This local etching behavior fits well with the final NPs showing patchiness of the Mg metal, with some areas intact.

Increasing the KAuCl$_4$ concentration relative to Mg NPs produces more decorations and increased coverage, which further support a galvanic mechanism (Figure 4A-F). The Mg K$_\alpha$ signal intensity in EDS decreases when a hexagonal nanoplate supports more Au decorations; eventually the particles can be seen to be fully oxidized (Figure S8). Meanwhile, the O K$_\alpha$ signal intensity in EDS remains essentially constant on the particles, suggesting a removal of the Mg metal and a constant, thermodynamically determined oxide layer thickness.

Figure 4.   Representative SEM images of Mg NPs decorated with Au NPs from different concentrations of KAuCl$_4$ (A: 0, B: 0.1, C: 0.2, D: 0.4, E: 0.6, F: 0.8 equivalents). G) Image of a Mg colloidal suspension with increasing molar equivalents of KAuCl$_4$, showing Mg NPs (0.0 eq) and Au-decorated Mg NPs (0.2-0.8 eq Au^{3+} : Mg^0) in ethanol. The total concentration of Mg in each vial is 1.2 mM. H) Extinction of Mg NPs and Au-decorated Mg NPs in ethanol.

The increase in Au decoration and corresponding decrease in Mg metal content is accompanied by a gradual modification of the plasmonic response of the particles. In completed reactions (Figure 4H), a band around 550 nm, characteristic of small Au NPs, rises in prominence with increasing Mg:Au ratio, together with a depression of the broad Mg-related resonances in the red region. Before the critical point for full replacement, i.e. below 0.66 Au molar equivalents (3 Mg^0 : 2 Au^{3+}), the nucleation of more Au NPs on the sacrificial template leads to a noticeable plasmonic coupling due to their confinement on a restrained environment. After this point, for instance at 0.8 equivalents, excess salt concentration and full oxidation of Mg causes aggregation of the decorated colloids, and a flat optical response is observed.

The scattering signature of decorated particles confirmed to be single by SEM also shows the expected modes from the addition of small Au NPs and their plasmonic coupling (peak ~ 500 nm), with a Mg mode still present at higher wavelength in some particles (Figure S9). The scattering signature of the bimetallic structures are notably stronger than that of the bare Mg NPs before galvanic replacement.

This signature plasmonic response can be exploited to follow the reaction kinetics, using a ratio of the LSPR wavelength of small particles of Au^0 (around 550 nm) and the Au^{3+} absorption band (at 340 nm). The reaction of 0.4 equivalents of Au salt with Mg NPs is reported in Figure S10, where a steady disappearance of the metal ion matches the rise of the Au NP plasmonic band over the ~3 hours necessary for the completion of the reaction.

C. DECORATION WITH OTHER METALS (Ag, Pd, Fe)

In order to further confirm that a galvanic replacement mechanism yields decorated, Mg-based architectures, other metals were introduced to the Mg colloidal suspensions, namely Ag, Pd, and Fe. Because of the low reduction potential of Mg,[27] metals less noble than Au can in principle be nucleated with Mg acting as the electron donor. When increasing the $AgNO_3$ concentration, we observed an increased LSPR response attributed to small Ag nanoparticles (around 420 nm) while the broad Mg LSPR band decreased throughout the visible range (Figure 5). After the critical point of 2 equivalents (2 Ag^+ per Mg^0), the steady increase of the 420 nm band stops and instead a collapse into a broad peak is observed, indicative of particle aggregation. This behavior is analogous to that described for $KAuCl_4$ and is as expected for a galvanic replacement mechanism. Since the reduction from Ag^+ to Ag requires only one electron compared to three for Au^{3+} to Au, we observe an increased amount of decorations with Ag on Mg NPs for a similar molar equivalent.

Figure 5.   HAADF-STEM images with A) high and B) low contrast for a Ag-decorated Mg

nanorod; the contrast change helps discern the underlying Mg scaffold. Scalebar,

100 nm. C) Image of a Mg colloidal suspension with increasing equivalence (eq) of

$AgNO_3$, showing Mg NPs (0.0 eq) and Ag-decorated Mg NPs (0.5-3.0 eq $Ag^+ : Mg^0$)

in ethanol. The total concentration of Mg in each vial is 1.2 mM. D) Extinction of

Mg NPs and Ag-decorated Mg NPs in ethanol.

In order to further substantiate the claim of a galvanic replacement mechanism, inductively

coupled plasma mass spectrometry (ICP-MS) was used to measure the amount of residual Mg left

in the NPs compared to the Mg^{2+} free in solution after the reaction (Figure 6). Samples with

different molar equivalents were centrifuged in ethanol and the clear supernatant was separated

from the centrifuged NPs. A 1% HNO_3 aqueous solution dissolved the Mg NP pellet almost

instantly; a proportional volume of diluted aqueous HNO_3 was added to the supernatant in order

to analyze the samples in identical matrices. A qualitative increase in solution-based Mg^{2+}

concentration was observed as more $AgNO_3$ was introduced, as expected from galvanic

replacement. Some Mg remains in the solids owing to the formation of non-soluble Mg oxide. This

ion concentration is also reflected in the morphology of the final products, where an increased

number of decorations (Figure S11) is present for an increasing Ag dose. The reaction kinetics for

Ag nucleation on Mg NPs were slower than that of Au, in part attributable to the electrochemical

differences between Mg and Ag vs. Mg and Au. For instance, the reaction of one molar equivalent

of $AgNO_3$ with Mg completed within approximately 24 hours (Figure S12).

Figure 6.   Relative Mg concentrations from pristine and Ag-decorated NPs (black marks) and from the supernatant (white marks) from ICP-MS. Error bars represent instrumental errors.

This versatile method can be adapted to decorate the interface of Mg NPs with other metals with a compatible reduction potential. Similar to the previous demonstration with Au and Ag which used $KAuCl_4$ and $AgNO_3$ salts, respectively, we have also managed to reduce small particles with different stoichiometry of $FeCl_3$ and Na_2PdCl_4 (Figure 7). Much like the plasmonic metals investigated earlier, the optical signature of the metals increases with the salt concentration introduced to the Mg NP suspension. However, since the decorations reduced from these salts are not expected to exhibit plasmonic properties, changes in the extinction spectra mainly result from higher energy interband absorption of these metals (Figure S13). MgFe – depending on the oxidized form of iron deposited in these architectures – and MgPd would provide two interesting compositions to further explore plasmon-activated catalysis in colloidal architectures.

Figure 7.   A) STEM-HAADF image of decorated MgPd NPs with 0.2 molar equivalent. B) Mg colloidal suspensions with increasing Na_2PdCl_4 equivalent, showing Mg NPs (0.0 eq) and Pd-decorated Mg NPs (0.2-1.2 eq Pd^{2+} : Mg^0) in ethanol. The total concentration of Mg in the 0.0 eq vial is 1.2 mM, while the decorated NPs were diluted by a factor of 5 with ethanol. C) TEM images of decorated MgFe NPs with 0.2 molar equivalent. D) Mg colloidal suspensions with increasing $FeCl_3$ equivalent, showing Mg NPs (0.0 eq) and Fe-decorated Mg NPs (0.2-0.8 eq Fe^{3+} : Mg^0) in ethanol. The total concentration of Mg is 1.2 mM in all vials.

D. MULTISTEP DECORATION OF Mg WITH Au AND Ag

The decoration by galvanic replacement also allows the reduction of a second salt on partially oxidized Mg NPs. To demonstrate this capability, we produced Mg NPs decorated by both Ag and Au (Figure 8). Their synthesis starts with Mg NPs and $KAuCl_4$, then the Au-decorated NPs are centrifuged, followed by an addition of $AgNO_3$ in ethanol leading to further galvanic replacement of the Mg. This sequence was chosen to eliminate galvanic replacement of Ag decorations by Au. The final extinction spectrum of the decorated colloids presents the LSPR bands of both Au (540 nm) and Ag (420 nm), over the broad background signal coming from leftover plasmonic Mg NPs. The signal from Ag in STEM-EDS is not spatially correlated with that of Au, suggesting that the added Ag decorations favor contact with the Mg/MgO surface over nucleation onto Au NPs. In Figure 8, the remaining Mg K_α signal is constant and low through the particle, while O K_α is also constant, indicating significant oxidation of the original Mg core after the successive galvanic replacement steps, starting with 0.5 molar equivalent of $KAuCl_4$ and then 0.1 equivalent of $AgNO_3$.

Figure 8. A) HAADF-STEM image of two Mg NPs decorated with Au and Ag NPs. Corresponding EDS maps of B) Au and Ag, and C) Mg and O. Scale bars, 100 nm. D) UV-Vis extinction spectra for Mg, MgAu, and MgAuAg NPs.

IV. CONCLUSIONS

We have demonstrated that partial galvanic replacement of Mg can be used to create bimetallic, decorated structures. This mechanism is supported by a plasmonic response through the UV-Vis-NIR wavelength range, ICP-MS data, SEM, STEM, and EDS maps that all show a decrease of Mg content and an increase of decoration when increasing the concentration of metal salt. We have shown that the low reduction potential of Mg allows it to be replaced by a wide range of metals such as (but not limited to) Au, Ag, Pd, and Fe. Partial galvanic replacement also means that residual Mg can be used to reduce other decorations in a multistep process, which forms, for instance, Mg NPs decorated by both Au and Ag. This provides an interesting platform for on-particle electrochemical reactions that do not involve the use of organic ligands and ensures that the particles are formed and immobilized on the host NP's surface. These decorations can be produced from virtually any metals, since the Mg reduction potential is much lower than that of most elements. Such architectures could be modified to integrate, at will, optical, catalytic and electronic properties via decoration with appropriate metals. These structures offer an exciting opportunity to investigate the coupling of Mg's recently demonstrated plasmonic properties with other better-established materials for plasmonic or photocatalysis applications.

V. SUPPLEMENTARY MATERIAL

See supplementary material for additional SEM images (including Mg size distribution), HAADF-STEM, STEM-EDS and STEM-EELS spectra and maps, DDA modelization, darkfield optical scattering spectra, UV-Vis absorption, and kinetics data.

VI. ACKNOWLEDGEMENTS

VII. REFERENCES

[1] C. Loo, A. Lin, L. Hirsch, M.H. Lee, J. Barton, N. Halas, J. West, and R. Drezek, Technol. Cancer Res. Treat. **3**, 33 (2004).

[2] P.L. Stiles, J.A. Dieringer, N.C. Shah, and R.P. Van Duyne, Annu. Rev. Anal. Chem **1**, 601 (2008).

[3] E. Fort and S. Grésillon, J. Phys. D. Appl. Phys. **41**, 013001 (2008).

[4] J.R. Lakowicz, K. Ray, M. Chowdhury, H. Szmacinski, Y. Fu, J. Zhang, and K. Nowaczyk, Analyst **133**, 1308 (2008).

[5] G. Baffou and R. Quidant, Chem. Soc. Rev. **43**, 3898 (2014).

[6] D.F. Swearer, H. Zhao, L. Zhou, C. Zhang, H. Robatjazi, J.M.P. Martirez, C.M. Krauter, S. Yazdi, M.J. McClain, E. Ringe, E.A. Carter, P. Nordlander, and N.J. Halas, Proc. Natl. Acad. Sci. U. S. A. **113**, 8916 (2016).

[7] J. Olson, A. Manjavacas, L. Liu, W.S. Chang, B. Foerster, N.S. King, M.W. Knight, P. Nordlander, N.J. Halas, and S. Link, Proc. Natl. Acad. Sci. U. S. A. **111**, 14348 (2014).

[8] X. Duan, S. Kamin, and N. Liu, Nat. Commun. **8**, 14606 (2017).

[9] J.N. Anker, W.P. Hall, O. Lyandres, N.C. Shah, J. Zhao, and R.P. Van Duyne, Nat. Mater. **7**, 442 (2008).

[10] B. Sepúlveda, P.C. Angelomé, L.M. Lechuga, and L.M. Liz-Marzán, Nano Today **4**, 244 (2009).

[11] M.G. Blaber, M.D. Arnold, and M.J. Ford, J. Phys. Condens. Matter **22**, 143201 (2010).

[12] P.B. Johnson and R.W. Christy, Phys. Rev. B **6**, 4370 (1972).

[13] M.W. Knight, N.S. King, L. Liu, H.O. Everitt, P. Nordlander, and N.J. Halas, ACS Nano **8**, 834 (2014).

[14] B.D. Clark, C.R. Jacobson, M. Lou, J. Yang, L. Zhou, S. Gottheim, C.J. DeSantis, P. Nordlander, and N.J. Halas, Nano Lett. **18**, 1234 (2018).

[15] B.D. Clark, C.J. DeSantis, G. Wu, D. Renard, M.J. McClain, L. Bursi, A.-L. Tsai, P. Nordlander, and N.J. Halas, J. Am. Chem. Soc. **141**, 1716 (2019).

[16] G.H. Chan, J. Zhao, G.C. Schatz, and R.P.V. Duyne, J. Phys. Chem. C **112**, 13958 (2008).

[17] G.H. Chan, J. Zhao, E.M. Hicks, G.C. Schatz, and R.P. Van Duyne, Nano Lett. **7**, 1947 (2007).

[18] S. Lu, H. Yu, S. Gottheim, H. Gao, C.J. Desantis, B.D. Clark, J. Yang, C.R. Jacobson, Z. Lu, P. Nordlander, N.J. Halas, and K. Liu, J. Am. Chem. Soc. **140**, 15412 (2018).

[19] S. Kim, J.-M. Kim, J.-E. Park, and J.-M. Nam, Adv. Mater. **30**, 1704528 (2018).

[20] B.D. Clark, C.R. Jacobson, M. Lou, D. Renard, G. Wu, L. Bursi, A.S. Ali, D.F. Swearer, A.-L. Tsai, P. Nordlander, and N.J. Halas, ACS Nano **13**, 9682 (2019).

[21] X. Duan and N. Liu, Acc. Chem. Res. **52**, 1979 (2019).

[22] Y. Gutierrez, D. Ortiz, J.M. Sanz, J.M. Saiz, F. Gonzalez, H.O. Everitt, and F. Moreno, Opt.

Express **24**, 20621 (2016).

[23] Y. Wang, E.M. Peterson, J.M. Harris, K. Appusamy, S. Guruswamy, and S. Blair, J. Phys. Chem. C **121**, 11650 (2017).

[24] F. Sterl, N. Strohfeldt, R. Walter, R. Griessen, A. Tittl, and H. Giessen, Nano Lett. **15**, 7949 (2015).

[25] J.S. Biggins, S. Yazdi, and E. Ringe, Nano Lett. **18**, 3752 (2018).

[26] W. Liu and K.-F. Aguey-Zinsou, J. Mater. Chem. A **2**, 9718 (2014).

[27] P. Vanýsek, in *Handb. Chem. Phys. 92nd Ed.* (2011), pp. 23–33.

[28] M.J. McClain, A.E. Schlather, E. Ringe, N.S. King, L. Liu, A. Manjavacas, M.W. Knight, I. Kumar, K.H. Whitmire, H.O. Everitt, P. Nordlander, and N.J. Halas, Nano Lett. **15**, 2751 (2015).

[29] G. Maidecchi, C.V. Duc, R. Buzio, A. Gerbi, G. Gemme, M. Canepa, and F. Bisio, J. Phys. Chem. C **119**, 26719 (2015).

[30] D. Renard, S. Tian, A. Ahmadivand, C.J. Desantis, B.D. Clark, P. Nordlander, and N.J. Halas, ACS Nano **13**, 3117 (2019).

[31] X. Li, H. Liu, J. Yang, S.Z. Qiao, and X.W. Du, RSC Adv. **4**, 1185 (2014).

[32] K.Y. Niu, S.A. Kulinich, J. Yang, A.L. Zhu, and X.W. Du, Chem. - A Eur. J. **18**, 4234 (2012).

[33] X. Xia, Y. Wang, A. Ruditskiy, and Y. Xia, Adv. Mater. **25**, 6313 (2013).

[34] L.M. Moreau, C.A. Schurman, S. Kewalramani, M.M. Shahjamali, C.A. Mirkin, and M.J. Bedzyk, J. Am. Chem. Soc. **139**, 12291 (2017).

[35] B.D. Anderson and J.B. Tracy, Nanoscale **6**, 12195 (2014).

[36] S.M. Rehn and E. Ringe, Part. Part. Syst. Charact. **35**, 1700381 (2018).

[37] P.R. Selvakannan and M. Sastry, Chem. Commun. **13**, 1684 (2005).

[38] Y. Yin, C. Erdonmez, S. Aloni, and A.P. Alivisatos, J. Am. Chem. Soc. **128**, 12671 (2006).

[39] X. Lu, H.Y. Tuan, J. Chen, Z.Y. Li, B.A. Korgel, and Y. Xia, J. Am. Chem. Soc. **129**, 1733 (2007).

[40] L. Polavarapu and L.M. Liz-Marzán, Nanoscale **5**, 4355 (2013).

[41] G. Collins, E.K. McCarty, and J.D. Holmes, CrystEngComm **17**, 6999 (2015).

[42] J. Yang, J.Y. Lee, and H.P. Too, J. Phys. Chem. B **109**, 19208 (2005).

[43] J. R. Daniel, L.A. McCarthy, E. Ringe, and D. Boudreau, RSC Adv. **9**, 389 (2019).

[44] M. Ahlers, Zeitschrift Für Phys. B Condens. Matter **99**, 491 (1996).

[45] S.H. Wei, A.A. Mbaye, L.G. Ferreira, and A. Zunger, Phys. Rev. B **36**, 4163 (1987).

[46] A. Kumar, E. Villarreal, X. Zhang, and E. Ringe, Adv. Struct. Chem. Imaging **4**, (2018).

[47] H. Okamoto and T.B. Massalski, Bull. Alloy Phase Diagrams **4**, 30 (1983).

[48] A.A. Nayeb-Hashemi and J.B. Clark, Bull. Alloy Phase Diagrams **5**, 348 (1984).

[49] R.H. Taylor, S. Curtarolo, and G.L.W. Hart, Phys. Rev. B **84**, 084101 (2011).

[50] L.D. Marks, Reports Prog. Phys. **57**, 603 (1994).

A) 500 nm

B) 100 nm

C) Mg / O — 100 nm

A) Mg O Au 100 nm

B) Mg O Au 100 nm

C) Mg O Au 100 nm

A)

100 nm

B)

MgO (2.1 Å)
Mg (3.0 Å)

Mg

MgO

10 nm

A) Mg (0 eq)

B) MgAu (0.1 eq)

C) MgAu (0.2 eq)

D) MgAu (0.4 eq)

E) MgAu (0.6 eq)

F) MgAu (0.8 eq)

G) 0.0 0.2 0.4 0.6 0.8 eq

H)

A) 100 nm

C) 250 nm 250 nm

B) 0.0 0.2 0.4 0.6 0.8 1.0 1.2 eq

D) 0.0 0.2 0.4 0.6 0.8 eq

Decoration of plasmonic Mg nanoparticles by partial galvanic replacement

Jérémie Asselin[1,2], Christina Boukouvala[1,2], Yuchen Wu[1], Elizabeth R. Hopper[1,2,3], Sean M. Collins[1], John S. Biggins[4], Emilie Ringe[1,2]*

1. Department of Materials Science and Metallurgy, University of Cambridge, Cambridge, United Kingdom, CB3 0FS
2. Department of Earth Sciences, University of Cambridge, Downing Street, Cambridge, United Kingdom, CB2 3EQ
3. Department of Chemical Engineering and Biotechnology, University of Cambridge, Cambridge, United Kingdom, CB3 0AS
4. Department of Engineering, University of Cambridge, Trumpington Street, Cambridge, United Kingdom, CB2 1PZ

* Corresponding author: er407@cam.ac.uk; +44 (0)1223 334300 (ph.), +44 (0)1223 334567 (fax).

Figure S1.   Histogram (108 NPs) of the tip-to-tip distance as measured in Mg hexagonal and truncated triangular plates, and nanorods. This size distribution has an average of 260 nm (standard deviation: 80 nm), and a thickness of 36 nm (standard deviation: 7 nm).
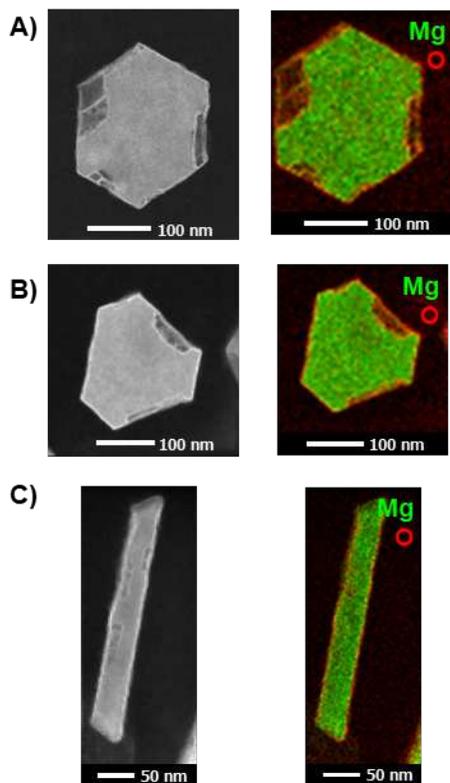
Figure S2.   Scanning transmission electronic microscopy (STEM) images and energy dispersive X-ray spectroscopy (EDS) maps of A) a hexagonal nanoplate, B) a truncated triangular nanoplate, C) and a nanorod.
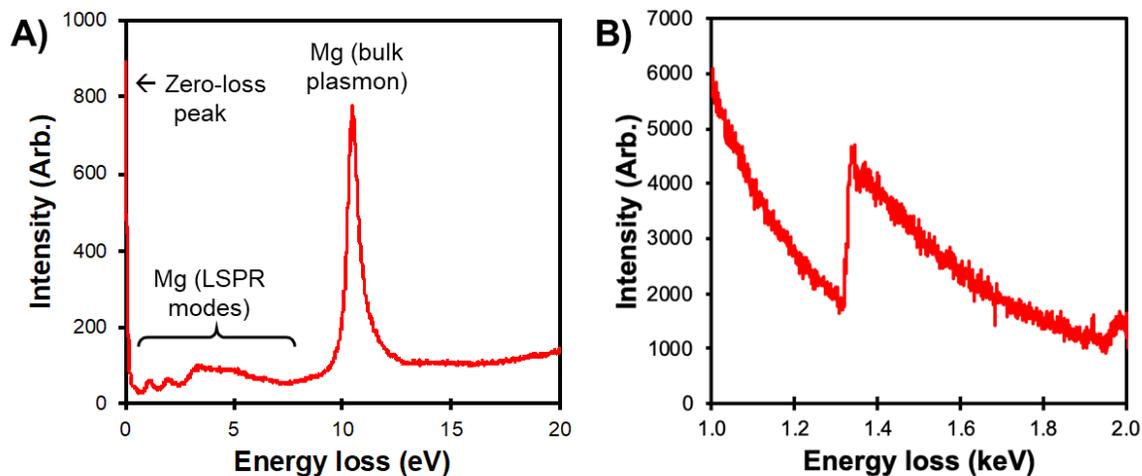
Figure S3.   A) Low-loss electron energy loss spectroscopy (STEM-EELS) data from the middle of a hexagonal nanoplate with an intense bulk Mg plasmon at 10.6 eV indicating the metallic nature of the Mg. B) Core-loss EELS spectrum of the Mg K-edge at 1.31 keV from the same Mg hexagonal nanoplate, consistent with metallic Mg.
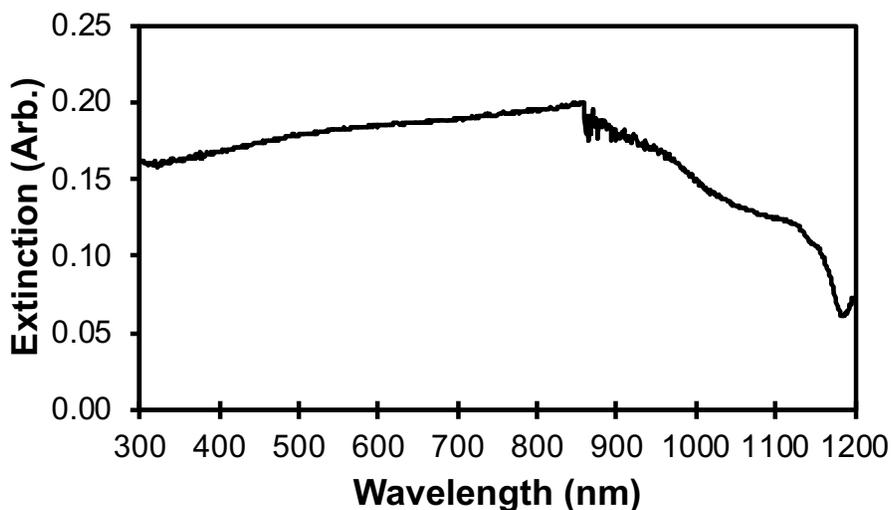
Figure S4.   UV-VIS extinction of Mg NPs suspended in anhydrous ethanol. The sharp spectral step-change feature and the increase of noise signal at 850 nm in the data were the result of a grating change in the instrument.
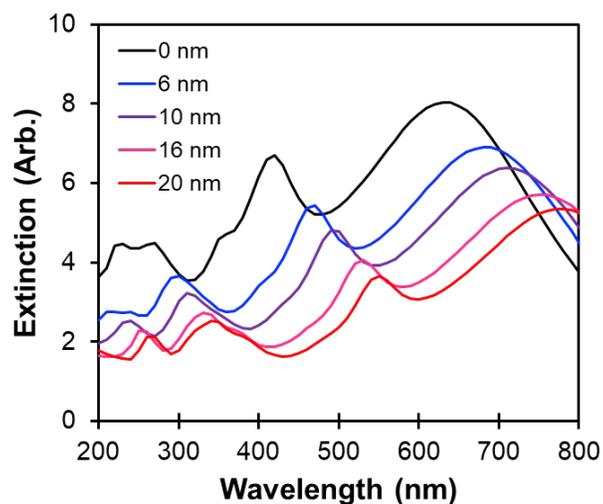
Figure S5. Computed extinction spectra for identical Mg hexagonal nanoplates coated with different thickness of MgO, demonstrating a 150 nm shift in the dipole resonance as a function of oxide thickness. Each calculation uses a 30 nm thick, 230 nm (tip-to-tip) Mg hexagonal plate, while the MgO coating thicknesses (given in the legend) span the experimentally observed range. The spectra are computed in the discrete dipole approximation using DDSCAT[1], with the lightbeam incident at 59º to the plate normal, reproducing the experimental conditions of the hyperspectral darkfield microscope used in the main paper. The refractive index of MgO was set to 1.7, the ambient refactive index was set to vacuum (*n* = 1.00), and the frequency dependent refractive index of metalic Mg was taken from Palick[2].
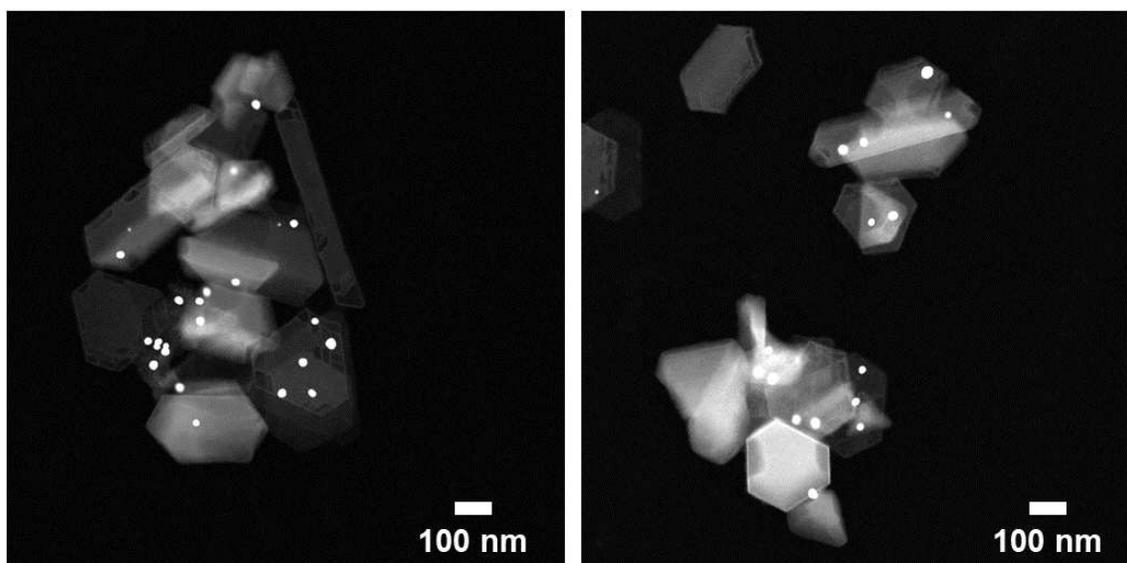
Figure S6. HAADF-STEM images of representative Au-decorated Mg NPs (0.1 equivalents) aggregates.
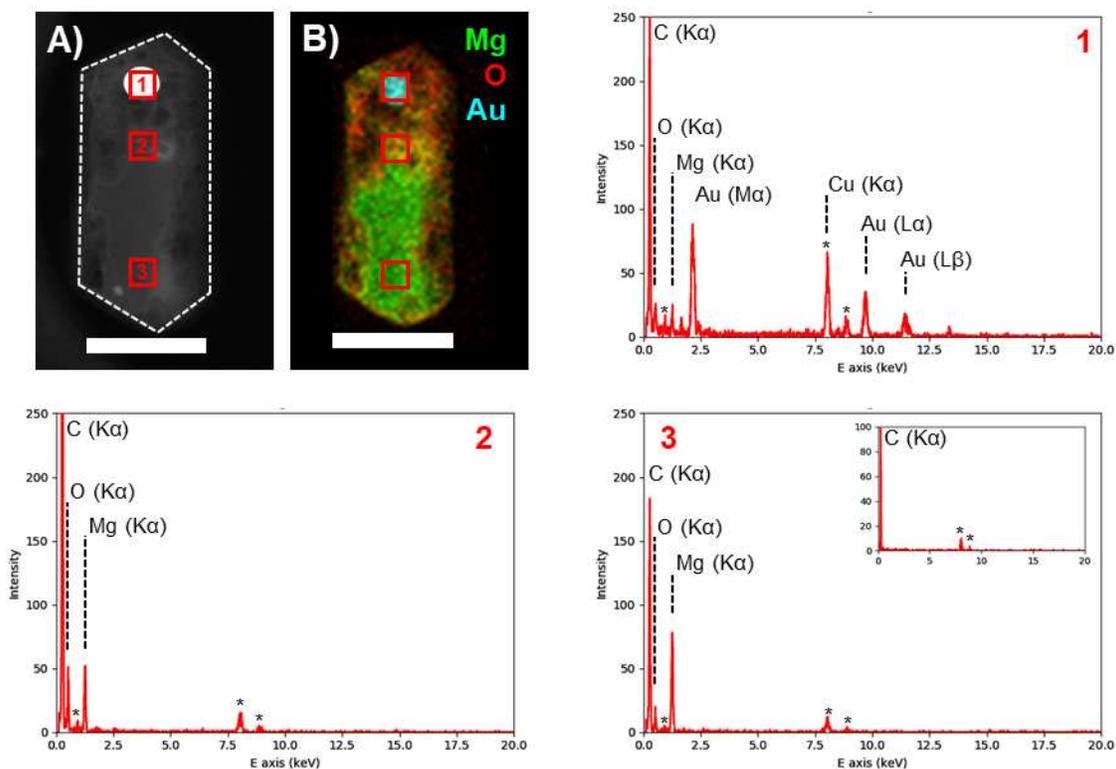
Figure S7.   HAADF-STEM image and EDS map presented in Figure 2 (main paper, scalebar, 100 nm) overlaid with 4×4 pixels regions of interest positioned 1) on the Au decoration, 2) at the edge of the oxidized Mg plate 3) at the non-oxidized tip of the NP. The background signal coming from the ultrathin carbon over lacey C on the Cu TEM grid is presented in the inset. EDS peaks assigned with an asterisk correspond to the Cu L_{α}, K_{α}, and K_{β} energies, which are associated with the Cu TEM grid used for the sample.
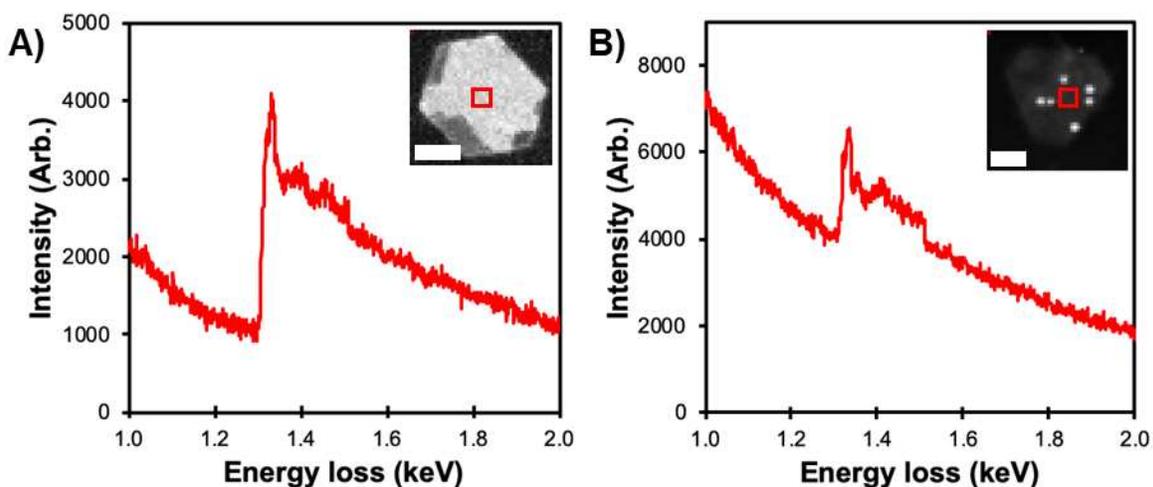
Figure S8.   EELS spectra showing the Mg K-edge changing from A) a hydrogenic shape for a bare Mg NP, and B) a sharp peak and delayed edge on a highly oxidized MgAu NP. Scalebars, 100 nm.
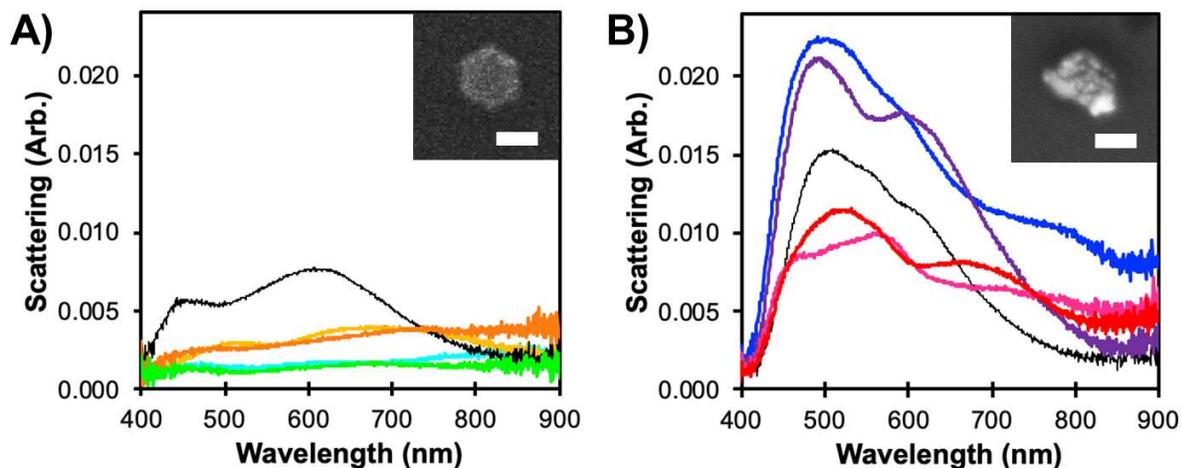
Figure S9.   Darkfield optical scattering signatures from A) bare Mg NPs and B) decorated MgAu NPs confirmed to be single by SEM mapping (typical NP presented in the respective insets). Scalebars, 200 nm.
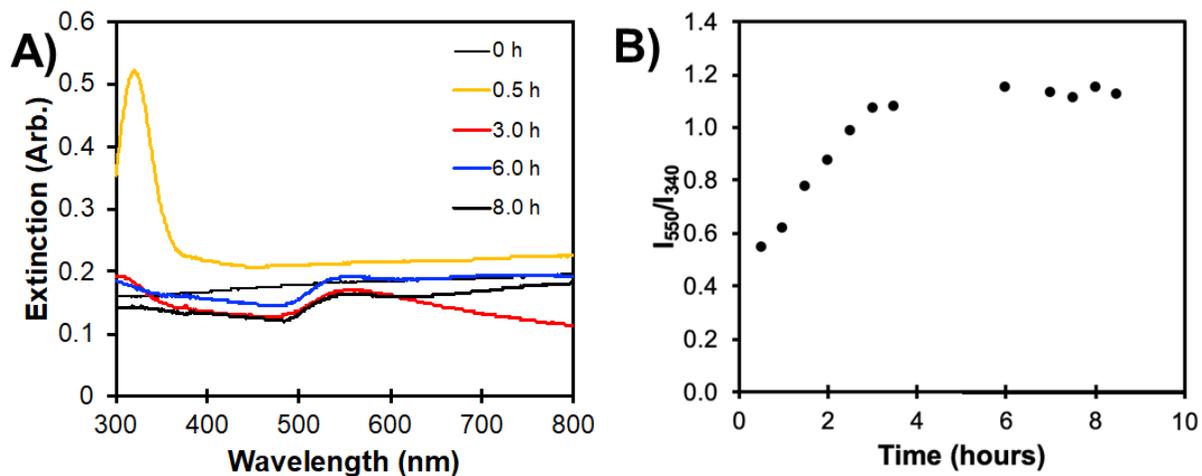
Figure S10. A) UV-VIS extinction spectra of Mg with 0.4 molar equivalents of KAuCl$_4$ in ethanol over an 8-hour period. B) Ratio of the LSPR band (550 nm) and Au^{3+} absorption (340 nm).
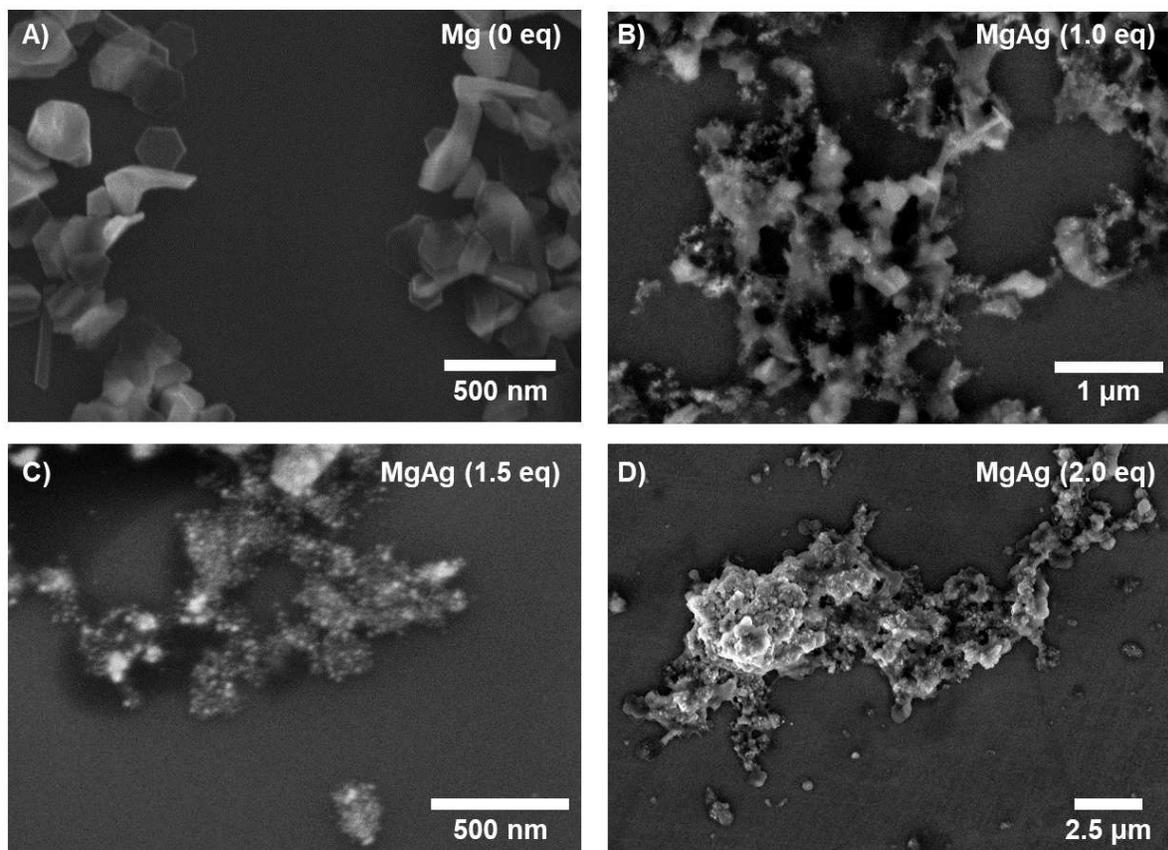
Figure S11. Representative SEM images of Mg NPs decorated with Ag with different molar equivalent of AgNO$_3$ (A: 0, B: 1.0, C: 1.5, D: 2.0 equivalents).
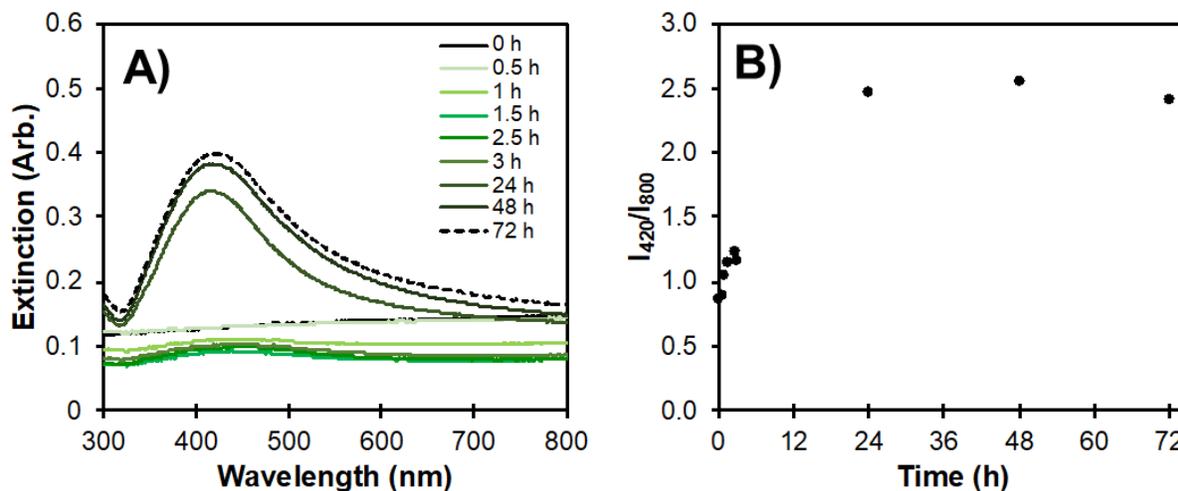
Figure S12. Reaction kinetics by UV-VIS extinction spectroscopy for the decoration of Mg NPs with AgNO$_3$. Mg concentration was 1.2 mM, with AgNO$_3$ concentration set at 1 molar equivalent (1 Mg : 1 Ag).
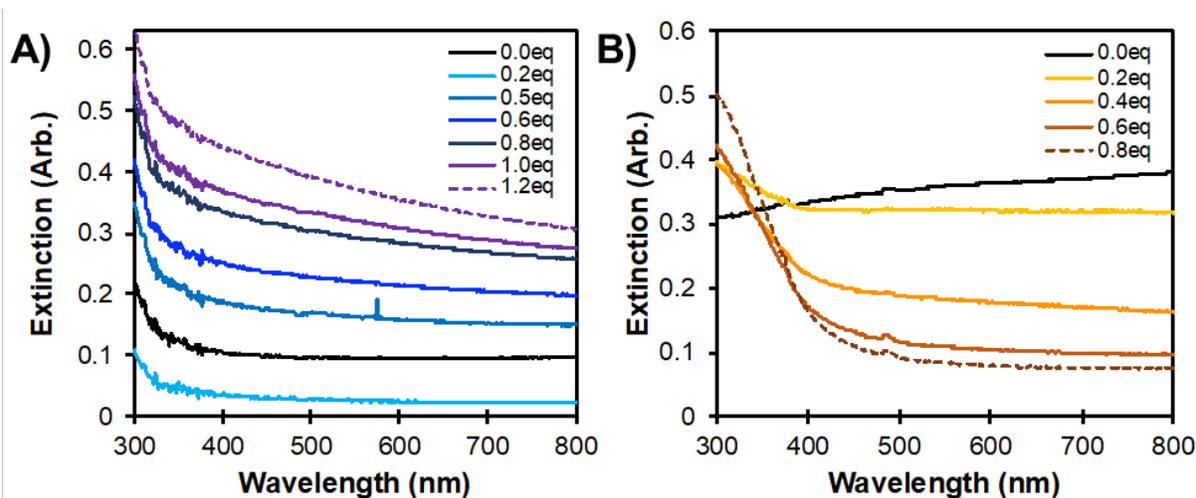
Figure S13. Post-reaction UV-VIS extinction spectra for Mg NPs colloidal suspensions with different equivalents of A) Na$_2$PdCl$_4$, B) FeCl$_3$.

REFERENCES

[1] B.T. Draine and P.J. Flatau, J. Opt. Soc. Am. **11**, 1491 (1994).
[2] E.D. Palik, *Handbook of Optical Constants of Solids*, Volume 3 (Cambridge, MA, 1998).